INORGANIC CHEMISTRY FRONTIERS

RESEARCH ARTICLE

View Article Online
View Journal | View Issue

Check for updates

Cite this: *Inorg. Chem. Front.*, 2025, **12**, 3997

Stepwise structural transformation in hybrid antimony chloride for time-resolved and multi-stage informational encryption and anti-counterfeiting†

Zeping Wang [a] and Xiaoying Huang *[b]

The growing issue of counterfeiting has driven an increasing demand for advanced anti-counterfeiting technologies. Stepwise structural transformations among numerous compounds offer a promising approach to achieving high-level anti-counterfeiting methods, such as multi-step and time-resolved techniques. However, research in this area is still in its early stages. In this work, we report the first example of the stepwise structural transformation from $ASbX_4$ (A = cation, X = halide) to A_2SbX_5 and further to A_3SbX_6. The compounds are $[Bzmim]_4[Sb_4Cl_{16}]$ (**1**, Bzmim = 1-benzyl-3-methylimidazolium), $[Bzmim]_2SbCl_5$ (**2**) and $[Bzmim]_3SbCl_6$ (**3**). **1**, **2**, and **3** exhibit distinct photoluminescent properties: non-emission, red emission peaking at 600 nm, and green emission peaking at 525 nm, respectively. Consequently, stepwise structural transformations enable stepwise luminescent switching from an "*off*" to multi-"*on*" states. Moreover, the switching mode can be adjusted from "*off-on*" to "*off-on*^{1}-*on*^{2}" by simply changing the reactant ratio. Using $SbCl_3$ ethanol solutions as invisible ink, multi-step and time-resolved information encryption and anti-counterfeiting were demonstrated by combining [Bzmim]Cl solution, UV light, time, and temperature as developers. The tunable composition and photoluminescent response modes of these IOMHs position them as excellent candidates for high-level information encryption and anti-counterfeiting applications. This work sheds light on the potential for developing advanced informational encryption technologies.

Received 23rd January 2025,
Accepted 25th March 2025

DOI: 10.1039/d5qi00256g

rsc.li/frontiers-inorganic

Published on 26 March 2025. Downloaded on 5/31/2026 6:15:04 AM.

Introduction

Information encryption is crucial in fields such as economics and the military. The advancement of cracking technologies has raised the bar for developing new encryption materials and techniques.[1] Among these, photoluminescent (PL) materials are particularly suitable for high-level information encryption and anti-counterfeiting due to their invisibility under normal conditions, rendering them uncopiable by conventional photocopiers.[1–6] To further extend the application of PL materials in information encryption and anti-counterfeiting, introducing time as a variable in the decryption process can significantly enhance security by increasing the difficulty of cracking encrypted information. For instance, information encoded using fluorescent and phosphorescent materials can be selectively read by observing different time intervals after switching excitation light off.[1,3–5] The combination of tunable PL properties, such as excitation wavelength and lifetime, enables multiple changes in information, facilitating higher-level encryption and anti-counterfeiting through increased complexity.[1] While extensively studied PL lifetime-based encryption methods demonstrate potential, differences in the response rates of stimuli-responsive PL materials, which alter their luminescent properties under external stimuli such as light, heat, or gases,[7,8] also offer time-dependent PL changes. For example, photo-induced structural transformation rate controlled by hydrogen bonding have been applied to time-resolved anti-counterfeiting.[9] However, most PL changes in stimuli-responsive materials occur only once. Achieving multi-step PL changes in such materials could greatly enhance information encryption levels, though research in this area remains limited.

Luminescent inorganic–organic hybrid metal halides (IOMHs) have recently garnered significant attention for their great advantages of chemical flexibility and straightforward

[a]*Hoffmann Institute of Advanced Materials, Shenzhen Polytechnic University, 7098 Liuxian Boulevard, Shenzhen, Guangdong 518055, P. R. China*
[b]*State Key Laboratory of Structural Chemistry, Fujian Institute of Research on the Structure of Matter, The Chinese Academy of Sciences, Fuzhou, Fujian, 350002, P. R. China. E-mail: xyhuang@fjirsm.ac.cn*

†Electronic supplementary information (ESI) available. CCDC 2415044. For ESI and crystallographic data in CIF or other electronic format see DOI: https://doi.org/10.1039/d5qi00256g

Published on 26 March 2025. Downloaded on 5/31/2026 6:15:04 AM.

preparation.[10–16] Represented by the general formula $A_aM_bX_c$ (where A is an organic cation, M is a metal ion, and X is a halide anion), IOMHs offer versatile design possibilities by varying cations, metal ions, halide anions, or their ratios.[11–15] Their ionic structures, characterized by weak interactions between cations and anions, contribute to structural resilience and high chemical reactivity. For example, Pb-,[17] Sn-,[18] Bi-,[19] Cu-,[20,21] Mn,[22] and Sb-based[23–25] IOMHs exhibit sensitivity to light, moisture, and other stimuli. Such responses, often caused by changes in the $A/M/X$ ratio, enhance the applicability of IOMHs in encryption and anti-counterfeiting due to their PL properties being closely tied to composition and structure.[26–32] Notable studies include Ma *et al.*'s report on the light-induced decomposition of Sn-IOMHs with the release of $SnBr_2$, leading to PL "*off-on*" switching,[18] and Zang *et al.*'s work demonstrating ethanol-triggered $(C_4NOH_{10})Cl$ release from Mn-IOMHs.[22] Song *et al.* reports the release of $(C_{19}H_{18}P)I$ induced structural transitions from $(C_{19}H_{18}P)_2CuI_3$ to $(C_{19}H_{18}P)_2Cu_4I_6$ for dynamically tunable emissions.[20] Our group has previously shown the controlled release of [PP14]Br from $[PP14]_2PbBr_4$ under heat.[33] These controlled release rates directly influence luminescent switching rate, enabling time-resolved luminescent information change. Importantly, IOMHs exhibit the potential for multi-step structural transformations due to the structural diversity of M_bX_c anions. For instance, Lei *et al.* reported stepwise structural changes from $[Ph_3EtP]_2Sb_2Cl_8$ to $[Ph_3EtP]_2SbCl_5{\cdot}EtOH$, and further to $[Ph_3EtP]_2SbCl_5$, resulting in a luminescent switching from non-emission to yellow-emission and finally to red-emission.[24] Despite these advancements, research on multi-step structural transformations and controlled component release in IOMHs remains in its infancy. Exploring stimuli-responsive IOMHs with multi-step structural and PL changes, combined with controlled release rates of AX and MX_n components, is essential for achieving high-level encryption techniques, such as time-resolved and multi-stage information encryption. This represents a promising yet underexplored avenue for advancing information encryption and anticounterfeiting technologies.

Herein, we report for the first time the stepwise structural transformation from $ASbX_4$ to A_2SbX_5 and further to A_3SbX_6. The compounds are $[Bzmim]_4[Sb_4Cl_{16}]$ (**1**, Bzmim = 1-benzyl-3-methylimidazolium), $[Bzmim]_2SbCl_5$ (**2**), and $[Bzmim]_3SbCl_6$ (**3**). Compound **1** exhibits no emission at room temperature, while **2** and **3** display red and yellow-green emissions under 390 nm UV light, respectively. These compounds can be selectively synthesized by varying the ratio of [Bzmim]Cl to $SbCl_3$. The conversion time from **1** to **2**, driven by the release rate of $SbCl_3$, can be tuned by adjusting the reactant ratio. As a result, a reactant ratio-controlled PL switching behavior was observed. When the [Bzmim]Cl to $SbCl_3$ ratio is less than 2, an "*off-on*" PL switching occurs, with the switching time decreasing as the ratio increases. When the ratio exceeds 2, an "*off-on*^{1}-*on*^{2}" switching is achieved, where the emission initially changes to red (**1** to **2**) and subsequently to yellow-green (**2** to **3**) upon further heat treatment. Using $SbCl_3$ solutions as invisible inks and [Bzmim]Cl solutions as developers, advanced encryption techniques were successfully demonstrated. This unique stepwise structural transformation behavior enables high-level information encryption and anti-counterfeiting applications based on the time-resolved and multi-stage PL changes, expanding the application scope of IOMHs in the field of information encryption and anti-counterfeiting.

Results and discussion

Structures and PL properties of the compounds. As shown in Fig. 1, the $[Sb_4Cl_{16}]^{4-}$ cluster contains 16 Cl^-, including two μ^3-Cl (Cl1) and four μ^2-Cl (Cl5 and Cl7) atoms, and the Sb–Cl distances range from 2.400 to 3.226 Å. Each $[Sb_4Cl_{16}]^{4-}$ cluster can be divided into two $[SbCl_4]^-$ anions, two $SbCl_3$ molecules, and two Cl^-, based on the typical Sb–Cl bond lengths, which mostly fall within the range of 2.1 to 2.8 Å.[23,24,34,35] In contrast, Sb–Cl bonds longer than 2.8 Å are considered secondary bonds. The secondary bonds result in weaker interactions compared to normal Sb–Cl bonds. In addition, both Sb1 and Sb2 exhibit distorted octahedral coordination geometries due to the larger bond length of secondary bond than normal bond. Unlike other zero-dimensional (0D) IOMHs, where the $[MX_y]^{n-}$ units are well-separated by counter cations,[10,12–14] the neighboring $[SbCl_n]^{3-n}$ units in **1** are connected by bridging Cl^- by secondary bonds. Besides the covalent and ionic bonds, abundant supramolecular interactions, including C–H···Cl hydrogen bonds and C–H···π interactions (as shown in Fig. S1†), contribute to the formation of a 3D supramolecular network structure.

Compounds **2** and **3** also feature 0D ionic structures, with cation-to-anion ratios of 2 : 1 and 3 : 1, respectively. The anions in **2** and **3** are $[SbCl_5]^{2-}$ and $[SbCl_6]^{3-}$, respectively. The Sb atoms exhibit a pyramidal penta-coordination geometry in **2** and an octahedral coordination geometry in **3** as shown in Fig. 1. In contrast to **1**, the $[SbCl_n]^{3-n}$ anions in **2** and **3** are fully separated from adjacent anions by the surrounding $[Bzmim]^+$ cations. Like **1**, supramolecular interactions are abundant in **2** and **3**, including C–H···Cl hydrogen bonds, π···π and C–H···π interactions, contributing to the formation of a 3D supramolecular network structure as shown in Fig. S2 and S3.†

Luminescent switching and accordingly structural transformation

As is well known, antimony(III) chloride units often act as the luminescent centres in Sb-IOMHs.[36–40] However, **1** is non-emissive at room temperature (RT), but exhibits red emission with a peak at 660 nm when cooled to 200 K (Fig. 2a), with a Stokes shift of 311 nm. At RT, the weak emission observed at 443 nm can be attributed to the emission of the $[Bzmim]^+$ cation.[41,42] As shown in Fig. 2b and c, **2** emits red light with a peak at 600 nm under excitation of UV light, while **3** emits yellow-green light with a peak at 525 nm. The excitation spectra reveal the absorption bands of **2** and **3** are respectively at 396 and 342 nm, corresponding to the $^1S_0 \rightarrow {}^3P_1$ transitions

 This journal is © the Partner Organisations 2025

Published on 26 March 2025. Downloaded on 5/31/2026 6:15:04 AM.

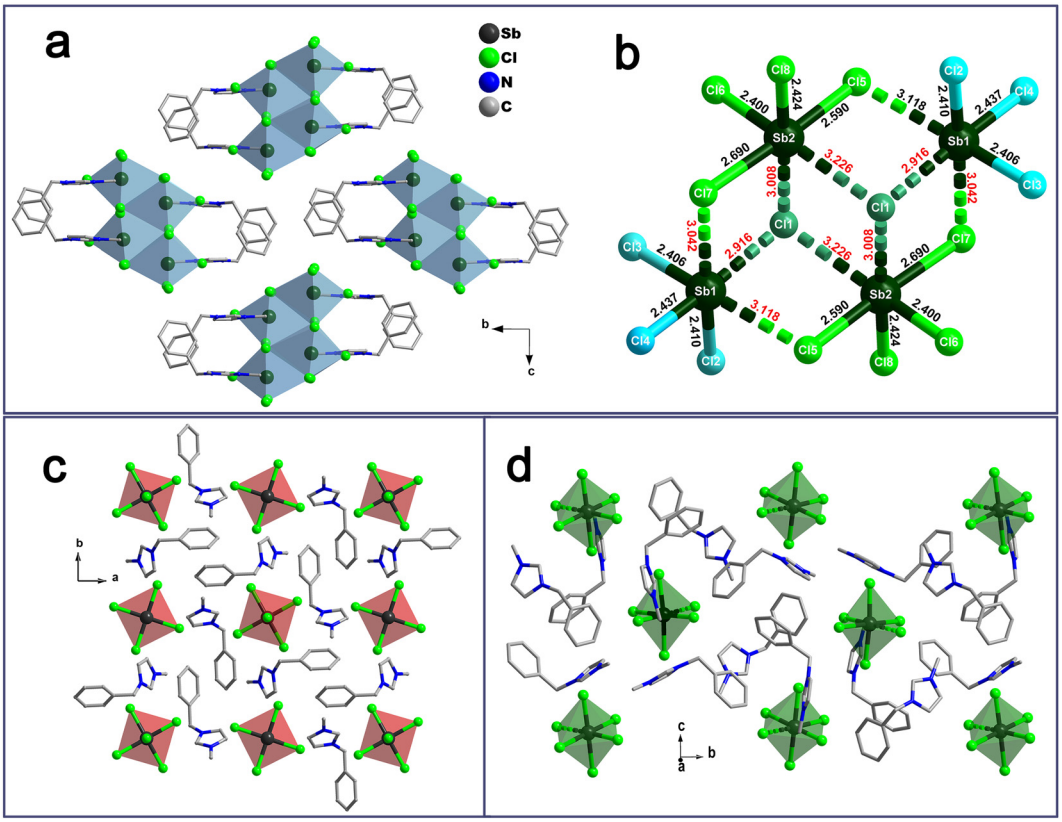

Fig. 1 (a) Crystal structure of **1** viewed along *a* axis. (b) Structure of $[Sb_4Cl_{16}]^{4-}$ cluster in **1**. (c) Crystal structure of **2** viewed along *c* axis. (d) Crystal structure of **3** viewed along *a* axis. H-atoms are omitted for clarity.

of Sb^{3+}.[43] The Stokes shifts for **2** and **3** are 204 nm and 183 nm, respectively, which are significantly smaller than that of **1** at 200 K. We also measured the PL quantum yield (PLQY) of **2** and **3** at RT. Under excitation wavelength of 375 nm, their PLQY values were determined to be 23% and 86%, respectively, aligning well fitted curves reveal that the PL lifetime of **2** and **3** at RT are both 2.3 μs. The μs-level lifetime aligns well with the previous report, further confirming that the PL of the materials origin from the energy transition between $^3P_1$ and $^1S_0$ of Sb^{3+}.[36–40]

To further study the mechanism behind the luminescent properties of the compounds, the distortion degrees of **1** and **3** were calculated using the formula below because their Sb^{3+} atoms have a same octahedral coordination geometry.

$$\Delta d = \left(\frac{1}{6}\right)\sum_{n=1}^{6}\left[\frac{d_n - d}{d}\right]^2$$

where d is the average Sb–Cl bond length and d_n are the six individual Sb–Cl bond lengths.[44] The average distortion degree of **1** and **3** is 0.0126 and 1.37×10^{-3}, respectively. In Sb-IOMHs, photoexcitation is accompanied by the transition of the s^2 ion from its ground state to an excited state with higher symmetry. Consequently, the degree of distortion in the environment of the Sb^{3+} in the ground state plays a critical role: the smaller the distortion degree, the lower the electron excitation energy required to transform the structure into the excited state (Fig. S5†). Conversely, as the distortion increases, the electron excitation energy also increases due to the slight shift of the excited-state parabola, as illustrated in Fig. S5.†[36,43,45] The ground state parabola may intersect with the excited state one in IOMHs with high distortion degree, leading to a lower luminescent quenching temperature, as observed in **1**. Furthermore, this shift in the excited-state parabola contributes to an increased Stokes shift, explaining why **1** exhibits a larger Stokes shift compared to **3**.

The distances between metal ions in hybrid ns^2 metal halide materials can also influence their PL properties.[46] The distances between neighbouring Sb atoms in **1** are 4.279, 4.252, and 4.560 Å, with the shortest value of 4.252 Å. For **2** and **3**, the minimum distances between Sb ions are 8.893 and 9.513 Å, respectively. These distances significantly influence the PL properties of the compounds through the concentration quenching effect.[10,47] Upon excitation, a migration process of the excitation energy through the lattice to quenching sites would occur,[47] which is energy transfer from $[SbCl_n]^{3-n}$ to $[SbCl_n]^{3-n}$ in title materials. The separation degree between Sb ions plays a pivotal role in this migration process, as the possibility of the process increases with the decreasing Sb···Sb distance.[47] Consequently, the Sb···Sb distance of 4.252 in **1**

Published on 26 March 2025. Downloaded on 5/31/2026 6:15:04 AM.

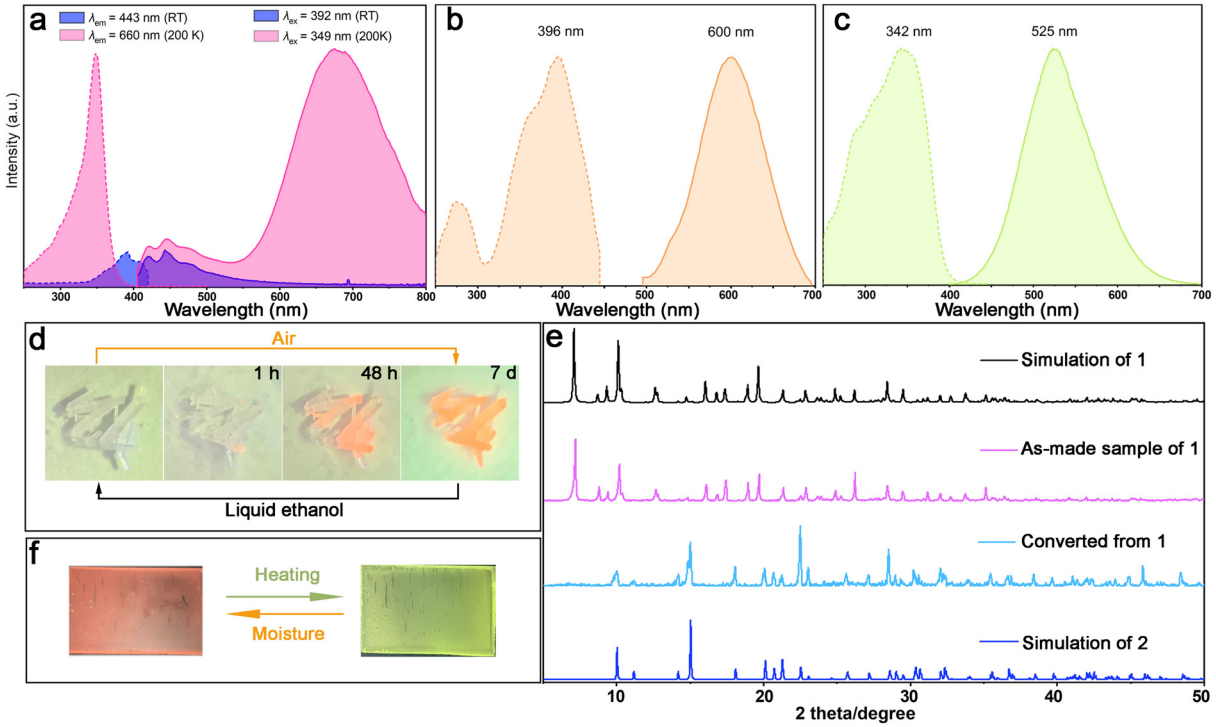

Fig. 2 Excitation (dotted lines) and emission (full lines) spectra of **1** (a), **2** (b), and **3** (c). (d) Images of single crystals of **1** under 390 nm UV light at different times. (e) Images of thin films of **2** (red one) and **3** (green one) under 390 nm UV light. (f) A comparation of the PXRD pattern between simulated and as-made sample of **1** before and after exposed in ambient condition.

results in non-emission property at RT. The migration process can be hampered at lower temperature, leading to the PL emission of **1** at 200 K. For **2** and **3**, the larger distances between Sb···Sb ions result in well-separated $SbCl_n^{3-n}$, enabling these compounds to exhibit favourable PL properties at RT.

Interestingly, when the single crystals of **1** was stored under ambient conditions, it was observed that the crystal turned light yellow after 7 days, accompanied by a luminescent change from non-emission to red emission, as shown in Fig. 2d. The single crystal was then ground into powder, and powder X-ray diffraction (PXRD) analysis was performed to identify the product. The PXRD pattern matched well with the simulated pattern of **2**, suggesting that the transformation from **1** to **2** occurred (Fig. 2e). Based on compositional and structural analysis of **1** and **2**, the transformation is likely due to the release of $SbCl_3$ from **1**. As described earlier, the $[Sb_4Cl_{16}]^{4-}$ cluster can be considered as comprising two $[SbCl_4]^-$ anions, two $SbCl_3$ units, and two Cl^- ions. The $SbCl_3$ units within **1** are weakly bonded to the surrounding $[Bzmim]^+$, $[SbCl_4]^-$, and Cl^-, allowing them to be released from the structure. Upon release of $SbCl_3$, the remaining Cl^- ions bond with the $[SbCl_4]^-$, forming $[Bzmim]_2SbCl_5$ (**2**), along with a change of PL properties. The framework of the single crystal of **1** remained intact after the structural transformation, highlighting its soft nature. The transformation time from **1** to **2** was found to depend on the degree of openness of the reaction system. In a closed system, the transformation from non-emissive white powder to red-emissive yellow powder occurred much more slowly than in an open system. As shown in Fig. S6,† the transformation of the powder of **1** in an open system was completed within ~3 hours, whereas it required ~15 hours in a closed system. Considering the volatility of $SbCl_3$ at RT, the unequal chemical potential between **1** and the surrounding air likely serves as the driving force for the transformation. Table 1 summarizes reported cases of *AX* or MX_n release-induced structural transformations in IOMHs, underscoring the novelty of this finding. In addition to the $SbCl_3$-release-induced structural transformation from **1** to **2**, it was discovered that immersing the powder of **2** in liquid ethanol for several days resulted in luminescence quenching. The PXRD pattern shown in Fig. S7† confirms that this phenomenon is caused by the reformation of **1**, likely due to the extraction of [Bzmim]Cl from **2**. This finding indicates that the structural transformation between **1** and **2** is reversible. A similar reversible phenomenon was observed between **2** and **3**. As shown in Fig. 2f, a reversible structural transformation between **2** and **3**, accompanied by PL switching between red and yellow-green emission, was noted. This transformation is attributed to the extraction and re-insertion of [Bzmim]Cl within the $[Bzmim]_{n-3}SbCl_n$ structure.[26] The extraction of [Bzmim]Cl from **3** can be triggered by exposure to moisture environment or liquid ethanol. Conversely, the re-insertion process can be achieved by either heating the **[Bzmim]Cl@2** mixture to a temperature below the melting point of **3** (410 K)

 This journal is © the Partner Organisations 2025

Published on 26 March 2025. Downloaded on 5/31/2026 6:15:04 AM.

Table 1 Summary of the structural transformation in IOMHs

Initial compound	Final compound	Stimulus	Released compound	Reversibility	Ref.
$(C_4N_2H_{14})SnBr_4$	$(C_4N_2H_{14}Br)_4SnBr_6$	Light	$SnBr_2$	No	18
$MAPbI_3$	MA_4PbI_6	H_2O	PbI_2	Yes	17
$(C_4NOH_{10})_5Mn_2Cl_9{\cdot}C_2H_5OH$	$(C_4NOH_{10})_2MnCl_4$	Heat	$(C_4NOH_{10})Cl$	No	22
$[PP14]_2[PbBr_4]$	$[PP14]_9[Pb_3Br_{11}][PbBr_4]_2$	Heat	[PP14]Br	Yes	33
$[DEDMA]_2SbCl_5$	$[DEDMA]_3Sb_2Cl_9$	H_2O	[DEDMA]Cl	Yes	48
$[Bzmim]_3SbCl_6$	$[Bzmim]_2SbCl_5$	H_2O	[Bzmim]Cl	Yes	26
$(TPA)CuBr_2$	$(TPA)_2Cu_4Br_6$	H_2O	(TPA)Br	Yes	21
$(C_{22}H_{24}P)_2SbCl_5$	$(C_{22}H_{24}P)_2Sb_2Cl_8$	Ethanol	$(C_{22}H_{24}P)Cl$	Yes	23
$(C_{19}H_{18}P)_2CuI_3$	$(C_{19}H_{18}P)_2Cu_4I_6$	MeOH	$(C_{19}H_{18}P)I$	Yes	20
$[Ph_3EtP]_2Sb_2Cl_8$	$[Ph_3EtP]_2SbCl_5{\cdot}EtOH$	EtOH	$SbCl_3$	No	24
$[Bzmim]_4[Sb_4Cl_{16}]$	$[Bzmim]_2SbCl_5$	Air	$SbCl_3$	Yes	This work

$C_4N_2H_{14}^{2+}$ = *N*,*N*′-dimethylethylenediaminium ion, MA^+ = methylamine ion, $C_4NOH_{10}^+$ = protonated morpholine, $PP14^+$ = *N*-butyl-*N*-methylpiperidinium, $DEDMA^+$ = diethyldimethyl ammonium, TPA^+ = tetrapropyl ammonium, $C_{22}H_{24}P^+$ = butyltriphenyl phosphonium, $C_{19}H_{18}P^+$ = methyltriphenyl phosphonium, Ph_3EtP^+ = ethyltriphenyl phosphonium.

or placing the mixture in a dryer at RT. Combining with the structural transformations from **2** to **1** in liquid ethanol environment, ethanol is effective in stepwise extracting [Bzmim]Cl from the $[Bzmim]_{n-3}SbCl_n$, enabling the stepwise structural transformations and luminescence switching among the three compounds.

Ratio-controlled PL switching rate and mode in Sb-IOMHs

Since the title compounds can all be synthesized from $SbCl_3$ and [Bzmim]Cl, the final product can be precisely controlled by adjusting the reactant ratio. Combined with the structural transformations among the three compounds, it is anticipated that altering the reactant ratio leads to controllable stimuli-responsive behavior driven by these potential structural transformations, thereby enabling tunable PL switching mode. To investigate the effect of reactant ratio on the resulting PL switching behavior, a series of ethanol solutions of [Bzmim]Cl and $SbCl_3$ were prepared and mixed in plastic vials. The $SbCl_3$ solution was added first, followed by the addition of [Bzmim]Cl in varying molar ratios as shown in Fig. 3a (see the experimental section for details). Immediately upon mixing, non-emissive white powder was generated, confirmed to be compound **1** by PXRD analysis as shown in Fig. S8.† The ethanol evaporated from the system within a few minutes, and the white powders of **1** gradually turned light yellow and began emitting red light under ambient conditions. The transformation time strongly correlated with the molar ratio of [Bzmim]Cl to $SbCl_3$; higher ratios resulted in shorter transformation times. For instance, powders with the highest [Bzmim]Cl/$SbCl_3$ ratio of 4 fully exhibited red emission within 0.5 hours, whereas those with the lowest ratio of 1 required approximately 3 hours to fully display red emission (Fig. 3a). PXRD patterns confirmed that **2** was the dominant product in all cases, responsible for the observed red luminescence. Interestingly, when the [Bzmim]Cl/$SbCl_3$ ratio exceeded 2.5, an additional emission color transition was observed. Upon heating the powders at 343 K, the red emission switched to yellow-green. PXRD analysis confirmed the formation of compound **3**, which was responsible for the yellow-green luminescence (Fig. S8†). Fig. 3b illustrates the stepwise structural transformations from $SbCl_3$ to $[Bzmim]_4[Sb_4Cl_{16}]$, $[Bzmim]_2SbCl_5$, and finally to $[Bzmim]_3SbCl_6$.

$$4SbCl_3 + 4[Bzmim]Cl \rightarrow [Bzmim]_4[Sb_4Cl_{16}] \quad (fast) \quad (1)$$

$$[Bzmim]_4[Sb_4Cl_{16}] \leftrightarrow 2[Bzmim]_2SbCl_5 + 2SbCl_3 \quad (slow) \quad (2)$$

$$[Bzmim]_2SbCl_5 + [Bzmim]Cl \leftrightarrow [Bzmim]_3SbCl_6 \quad (slow) \quad (3)$$

The stepwise structural transformation and corresponding multi-step PL switching provide valuable insights into the reaction mechanism underlying the synthesis of Sb(III) based

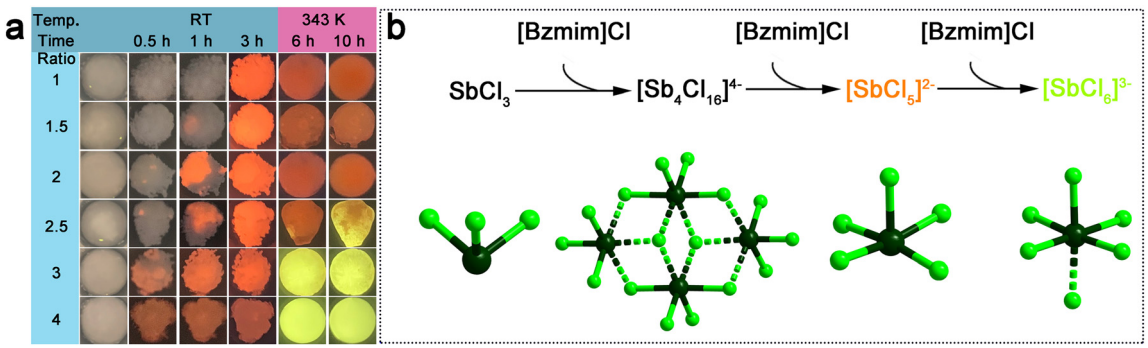

Fig. 3 (a) Digital pictures of a series of powders after mixing the reactants (under 390 nm UV light). (b) Demonstration of the reaction processes after mixing the reactants (light green ball: Cl atom; dark green ball: Sb atom).

Published on 26 March 2025. Downloaded on 5/31/2026 6:15:04 AM.

IOMHs. When the ratio of [Bzmim]Cl to $SbCl_3$ decreases, excess $SbCl_3$ remains in the reaction system. The limited availability of Cl^- ions prevents the formation of isolated anions such as $[SbCl_5]^{2-}$ and $[SbCl_6]^{3-}$. Consequently, the tetrameric structure of $[Sb_4Cl_{16}]^{4-}$-based material is formed (formula (1)), which exhibits non-emissive properties at RT. Over time, compound **1** gradually transforms into the red-emissive compound **2**, as represented in formula (2). This transformation is driven by the release of $SbCl_3$, which reacts with [Bzmim]Cl when excess [Bzmim]Cl is present in the system, ultimately forming $[Bzmim]_2SbCl_5$ (**2**) until the [Bzmim]Cl is completely consumed. Although the reaction involves $SbCl_3$ release, the process resembles the insertion of [Bzmim]Cl into **1** to produce **2**. When the [Bzmim]Cl/$SbCl_3$ ratio exceeds 2, further [Bzmim]Cl insertion occurs into **2**, resulting in the formation of compound **3** after heat treatment. This stepwise transformation causes the emission color of the powders to switch from red to yellow-green. Thus, the insertion of [Bzmim]Cl into $SbCl_3$ proceeds in a stepwise manner as shown in Fig. 3b, enabling the sequential formation of **1**, **2**, and **3**. The reverse processes, involving the extraction of [Bzmim]Cl, can also be achieved in a stepwise fashion. Placing the green-emissive powder of **3** in a moist environment triggers the initial extraction of [Bzmim]Cl, resulting in a PL color switch back to red, corresponding to compound **2**. Subsequent addition of liquid ethanol completes the transformation to the non-emissive compound **1**, as the PL switches from red to non-emission.

Time-resolved and multi-steps information encryption based on Sb-IOMHs

The reactant ratio-controlled PL switching, coupled with tunable switching rates, supports time-resolved information encryption and advanced anticounterfeiting strategies. To meet the demand for confidential information encryption, selecting a suitable composite for invisible ink is crucial. Typically, one of the components used in the synthesis of IOMHs can serve as the invisible ink, while another component acts as the developer. For example, Li *et al.* reported the transformation of an invisible Pb-MOF (metal–organic framework) into a composite of luminescent $MAPbBr_3$ nano crystals and Pb-MOF by employing Pb-MOF as the invisible ink and MABr as the developer.[49] Similarly, Xia *et al.* demonstrated a MABr-triggered information decryption process using $PbBr_2$ containing lanthanide MOFs as invisible ink.[50] Sun *et al.* explored full-color information encryption by combining halide salts with $CsPbCl_3$ quantum dots as the invisible ink and developer, respectively.[51] They also introduced selective information display through additional water treatment as a developer. In another study, they used composites of Cs_4PbBr_6 and $CsPbCl_3$, as well as $CsPbBr_3$ nanoplatelets, as invisible inks for multi-functional encryption.[52] However, the high compositional tunability of such materials family has rarely been utilized for information encryption and anti-counterfeiting. The controllable reaction rates and PL. switching behaviors of the $[Bzmim]_{n-3}SbCl_n$ series materials offer unique potential for time-resolved and multi-step information encryption. This introduces "time" as an additional developer, providing an innovative pathway for enhancing the security and functionality of anti-counterfeiting measures and confidential information storage.

Fig. 4a illustrates the details of the invisible ink, developers, and the fabrication strategy for the multi-step and time-resolved information encryption process. Initially, confidential messages written with varying concentrations of $SbCl_3$ ink are completely invisible under both visible light and UV light. Upon applying [Bzmim]Cl ink at a specific concentration to the entire paper, red-emissive information gradually appears under a UV lamp, corresponding to the structural transformation from compound **1** to **2**. The true information can be concealed within letters like "H", "HI", "HIA", or "HIAM". Heating the paper at high temperatures induces the transformation from compound **2** to **3**, revealing the letters "HI" and "AM", designed to confuse potential adversaries with false messages. The authentic information remains hidden unless [Bzmim]Cl ink with the correct concentration is applied, and the message is observed at the appropriate time and temperature.

As a proof of concept, a series of circular filter papers (5 mm in diameter), coated with invisible $SbCl_3$ inks of different concentrations, were prepared and arranged as shown in Fig. 4b. The PL "*off*" and "*on*" states are respectively defined as "0" and "1" in a binary system. Upon applying [Bzmim]Cl solution of uniform concentration, the information transitions to "41 601" after 5 minutes, "48 097" after 10 minutes, and "65 535" after 30 minutes. This demonstrates time-resolved information changes driven by the concentration-dependent rate of structural transformation. Interestingly, in contrast to the observations in plastic vials, the filter paper experiments showed that red emission first appeared in samples with the highest $SbCl_3$ concentration, rather than those with the highest [Bzmim]Cl/$SbCl_3$ ratio (Fig. 4b). This discrepancy may be attributed to the overwhelming presence of [Bzmim]Cl in the reaction system on the filter paper. As a result, the reaction rate was primarily governed by the amount of $SbCl_3$ available, rather than the reactant ratio. This phenomenon was further observed in another experiment, where a letter was written on paper using $SbCl_3$ solutions at specific concentrations (details provided in Fig. 4c). Initially, the letter "L" becomes visible under UV light by emitting red luminescence. An adversary attempting to decode the information may stop at this stage, mistaking it for the true message. However, as time progresses, the letter transitions to "C" and eventually to "O", revealing the actual message. Notably, the decryption process is single-use. Any attempt to uncover the hidden information leaves an irreversible mark, providing an additional layer of security by alerting the user that the information decryption has been tampered with.

For the multi-stage information encryption and anti-counterfeiting demonstration, the word "disagree" was selected to be written on the paper (Fig. 4d, detailed in the experimental section). The correct decryption process requires the following steps: (1) drop a [Bzmim]Cl solution of a specific concentration onto the paper; (2) heat the paper to a specific temperature

 This journal is © the Partner Organisations 2025

Published on 26 March 2025. Downloaded on 5/31/2026 6:15:04 AM.

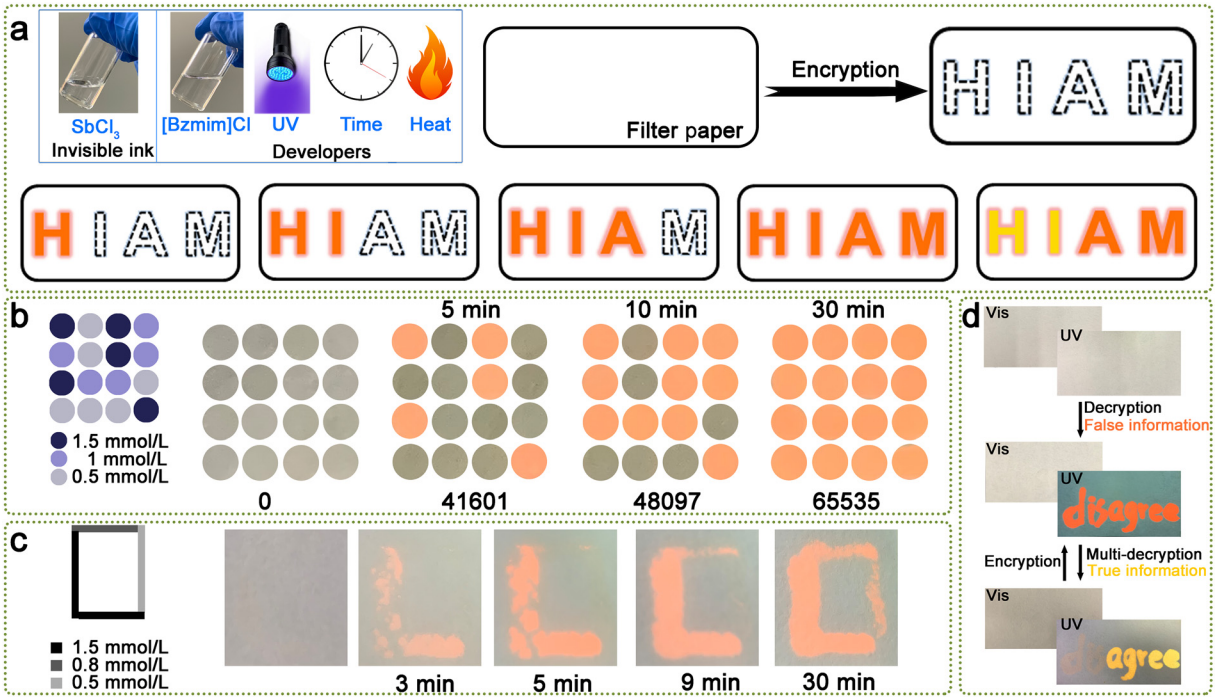

Fig. 4 (a) Demonstration of the multi-step and time-resolved decryption processes of information, the insert image shows the invisible ink and developers. (b) Digital pictures of the filter paper coated by [Bzmim]Cl and $SbCl_3$ solutions with different concentrations (under 390 nm UV light) at different time. (c) Digital pictures of the written letter on a filter paper before and after decryption under 390 nm UV lamp at different time. (d) Digital pictures of the paper before and after heating with the words written by [Bzmim]Cl and $SbCl_3$ inks (under 390 nm UV light).

and (3) observe it under a UV lamp. After the first step, the word "disagree" becomes visible under UV light, emitting red luminescence. However, this is false information. To reveal the true message, a secondary developer (heat) must be applied. Upon heating at 80 °C for 30 min, the true message, "agree", emerges under UV light. The concentration of the [Bzmim]Cl solution plays a critical role in this process. If the concentration is too low, there will be insufficient [Bzmim]Cl on the paper to trigger the structural transformation, leaving the information hidden. Conversely, if the concentration is too high, an excess of [Bzmim]Cl on the paper leads to all the letters emitting yellow-green light under UV illumination after heating, still displaying the false information. The interplay between the concentration of developer and the structural transformation is crucial for revealing the correct information at the appropriate stage, adding complexity and security to the decryption process. Recently, there are some advances in multi-stage informational encryption and anti-counterfeiting using single-component multimode luminescent metal halides.[53–55] For example, Xia *et al.* demonstrated multiple encryption using excitation-dependent multi-excitonic emission in $ATPP_2SnCl_6:Sb^{3+}$.[53] They also integrated self-trapped excitons, dopants, and defects within a single-component luminescent material to achieve multimode luminescence for multilevel anti-counterfeiting.[54] By contrast, our study presents a novel approach based on controllable structural transformations among multiple components. This approach facilitates tunable multimode luminescence through multi-component transformations, surpassing the commonly reported structural transformations between two components.

Conclusions

In conclusion, a reversible structural transformation from $[Bzmim]_4[Sb_4Cl_{16}]$ to $[Bzmim]_2SbCl_5$ and further to $[Bzmim]_3SbCl_6$ was reported, resulting in a PL switching among non-emission, red-emission and yellow-green emission. This demonstrates the first example of multi-step reversible structural transformations from $ASbX_4$ to A_2SbX_5 and further to A_3SbX_6 in IOMHs. Additionally, reactant ratio-controlled PL switching modes were investigated, transitioning from a simple "*off-on*" mode to a novel "*off-on*^{1}-*on*^{2}" mode. Using $SbCl_3$ ethanol solutions of varying concentrations as invisible ink, and the combination of [Bzmim]Cl solution, UV light, time, and temperature as developers, multi-step, time-resolved information encryption and anticounterfeiting was achieved. The tunable composition and PL-responsive behavior of these IOMHs position them as excellent candidates for high-level information encryption and anticounterfeiting applications. This work highlights the potential of stimuli-responsive IOMHs in advancing information protection technologies and paves the way for exploring new functional materials in this field.

Published on 26 March 2025. Downloaded on 5/31/2026 6:15:04 AM.

Author contributions

Zeping Wang: conceptualization, data curation, formal analysis, funding acquisition; investigation, methodology, writing – original draft, writing – review & editing; Xiaoying Huang: funding acquisition, project administration, supervision, writing – review & editing.

Data availability

All data needed to evaluate the conclusions in the paper are present in the paper and/or the ESI.† X-ray crystallographic data for $[Bzmim]_4[Sb_4Cl_{16}]$ (CCDC 2415044†) is available in https://www.ccdc.cam.ac.uk/.

Conflicts of interest

There are no conflicts to declare.

Acknowledgements

We thank the financial supports from the National Nature Science Foundation of China (No. 22205236 and 92261115) and the Natural Science Foundation of Fujian Province (No. 2022J05089).

References

1 X. W. Yu, H. Y. Zhang and J. H. Yu, Luminescence Anti-counterfeiting: From Elementary to Advanced, *Aggregate*, 2021, **2**, 20–34.
2 Z. Sun, J. Yang, L. Huai, W. Wang, Z. Ma, J. Sang, J. Zhang, H. Li, Z. Ci and Y. Wang, Spy Must Be Spotted: A Multistimuli-Responsive Luminescent Material for Dynamic Multimodal Anticounterfeiting and Encryption, *ACS Appl. Mater. Interfaces*, 2018, **10**, 21451–21457.
3 K. Jiang, Y. Wang, C. Cai and H. Lin, Conversion of Carbon Dots from Fluorescence to Ultralong Room-Temperature Phosphorescence by Heating for Security Applications, *Adv. Mater.*, 2018, **30**, e1800783.
4 Z. Tian, D. Li, E. V. Ushakova, V. G. Maslov, D. Zhou, P. Jing, D. Shen, S. Qu and A. L. Rogach, Multilevel Data Encryption Using Thermal-Treatment Controlled Room Temperature Phosphorescence of Carbon Dot/Polyvinylalcohol Composites, *Adv. Sci.*, 2018, **5**, 1800795.
5 Y. Su, S. Z. F. Phua, Y. Li, X. Zhou, D. Jana, G. Liu, W. Q. Lim, W. K. Ong, C. Yang and Y. Zhao, Ultralong room temperature phosphorescence from amorphous organic materials toward confidential information encryption and decryption, *Sci. Adv.*, 2018, **4**, eaas9732.
6 J.-Q. Zhao, H.-S. Shi, L.-R. Zeng, H. Ge, Y.-H. Hou, X.-M. Wu, C.-Y. Yue and X.-W. Lei, Highly emissive zero-dimensional antimony halide for anti-counterfeiting and confidential information encryption-decryption, *Chem. Eng. J.*, 2022, **431**, 134336.
7 Z. P. Wang and X. Y. Huang, Luminescent Organic-Inorganic Hybrid Metal Halides: An Emerging Class of Stimuli-Responsive Materials, *Chem. – Eur. J.*, 2022, **28**, e202200609.
8 Y. J. Huang, L. J. Ning, X. M. Zhang, Q. Zhou, Q. Y. Gong and Q. C. Zhang, Stimuli-fluorochromic Smart Organic Materials, *Chem. Soc. Rev.*, 2024, **53**, 1090–1166.
9 Y. Xie, X. Zhao, H. Wang, Y. Tian, C. Liu, J. Wu, J. Cui, Z. Zhou, J. Chen and X. Chen, Hydrogen Bond-Associated Photofluorochromism for Time-Resolved Information Encryption and Anti-counterfeiting, *Angew. Chem., Int. Ed.*, 2024, e202414846.
10 K. M. McCall, V. Morad, B. M. Benin and M. V. Kovalenko, Efficient Lone-Pair-Driven Luminescence: Structure-Property Relationships in Emissive 5s(2) Metal Halides, *ACS Mater. Lett.*, 2020, **2**, 1218–1232.
11 S. L. Wang, F. Yang, J. R. Zhu, Q. X. Cao, Y. G. Zhong, A. C. Wang, W. N. Du and X. F. Liu, Growth of Metal Halide Perovskite Materials, *Sci. China Mater.*, 2020, **63**, 1438–1463.
12 J. C. Jin, N. N. Shen, Z. P. Wang, Y. C. Peng and X. Y. Huang, Photoluminescent Ionic Metal Halides Based on s(2) Typed Ions and Aprotic Ionic Liquid Cations, *Coord. Chem. Rev.*, 2021, **448**, 214185.
13 M. Z. Li and Z. G. Xia, Recent Progress of Zero-dimensional Luminescent Metal Halides, *Chem. Soc. Rev.*, 2021, **50**, 2626–2662.
14 C. K. Zhou, L. J. Xu, S. J. Lee, H. R. Lin and B. W. Ma, Recent Advances in Luminescent Zero-Dimensional Organic Metal Halide Hybrids, *Adv. Opt. Mater.*, 2021, **9**, 2001766.
15 A. Fakharuddin, M. K. Gangishetty, M. Abdi-Jalebi, S. H. Chin, A. B. Yusoff, D. N. Congreve, W. Tress, F. Deschler, M. Vasilopoulou and H. J. Bolink, Perovskite Light-emitting Diodes, *Nat. Electron.*, 2022, **5**, 203–216.
16 K. Han, J. C. Jin, B. B. Su and Z. G. Xia, Molecular Dimensionality and Photoluminescence of Hybrid Metal Halides, *Trends Chem.*, 2022, **4**, 1034–1044.
17 J. A. Christians, P. A. Miranda Herrera and P. V. Kamat, Transformation of the excited state and photovoltaic efficiency of $CH_3NH3PbI3$ perovskite upon controlled exposure to humidified air, *J. Am. Chem. Soc.*, 2015, **137**, 1530–1538.
18 C. Zhou, Y. Tian, M. Wang, A. Rose, T. Besara, N. K. Doyle, Z. Yuan, J. C. Wang, R. Clark, Y. Hu, T. Siegrist, S. Lin and B. Ma, Low-Dimensional Organic Tin Bromide Perovskites and Their Photoinduced Structural Transformation, *Angew. Chem., Int. Ed.*, 2017, **56**, 9018–9022.
19 O. Toma, M. Allain, F. Meinardi, A. Forni, C. Botta and N. Mercier, Bismuth-Based Coordination Polymers with Efficient Aggregation-Induced Phosphorescence and Reversible Mechanochromic Luminescence, *Angew. Chem., Int. Ed.*, 2016, **55**, 7998–8002.
20 R. An, Q. Wang, Y. Liang, P. Du, P. Lei, H. Sun, X. Wang, J. Feng, S. Song and H. Zhang, Reversible Structural Phase

 This journal is © the Partner Organisations 2025

Published on 26 March 2025. Downloaded on 5/31/2026 6:15:04 AM.

Transitions in Zero-Dimensional Cu(I)-Based Metal Halides for Dynamically Tunable Emissions, *Angew. Chem., Int. Ed.*, 2024, e202413991.

21 Y. Tian, H. Peng, Q. Wei, Y. Chen, J. Xia, W. Lin, C. Peng, X. He and B. Zou, Moisture-Induced reversible structure conversion of Zero-Dimensional organic cuprous bromide hybrids for multiple photoluminescent anti-Counterfeiting, information encryption and rewritable luminescent paper, *Chem. Eng. J.*, 2023, **458**, 141436.

22 M. E. Sun, Y. Li, X. Y. Dong and S. Q. Zang, Thermoinduced structural-transformation and thermochromic luminescence in organic manganese chloride crystals, *Chem. Sci.*, 2019, **10**, 3836–3839.

23 Z. Zang, D. Liang, Y. Shi, Z. Liu, R. Li, S. M. H. Qaid and W. Cai, Ethanol-Induced Reversible Phase Transition in Antimony Halides for Morse Code Anti-Counterfeiting and Optical Logic Gates, *Laser Photonics Rev.*, 2024, 2401304.

24 J.-Q. Zhao, Y.-Y. Ma, X.-J. Zhao, Y.-J. Gao, Z.-Y. Xu, P.-C. Xiao, C.-Y. Yue and X.-W. Lei, Stepwise Crystalline Structural Transformation in 0D Hybrid Antimony Halides with Triplet Turn-on and Color-Adjustable Luminescence Switching, *Research*, 2023, **6**, 0094.

25 D.-Y. Li, J.-H. Song, Y. Cheng, X.-M. Wu, Y.-Y. Wang, C.-J. Sun, C.-Y. Yue and X.-W. Lei, Ultra-Sensitive, Selective and Repeatable Fluorescence Sensor for Methanol Based on a Highly Emissive 0D Hybrid Lead-Free Perovskite, *Angew. Chem., Int. Ed.*, 2022, **61**, e202206437.

26 Z. Wang, Z. Zhang, L. Tao, N. Shen, B. Hu, L. Gong, J. Li, X. Chen and X. Huang, Hybrid Chloroantimonates(III): Thermally Induced Triple-Mode Reversible Luminescent Switching and Laser- Printable Rewritable Luminescent Paper, *Angew. Chem., Int. Ed.*, 2019, **58**, 9974–9978.

27 X. Chen, F. Zhang, Y. Ge, L. Shi, S. Huang, J. Tang, Z. Lv, L. Zhang, B. Zou and H. Zhong, Centimeter-Sized Cs_4PbBr_6 Crystals with Embedded $CsPbBr_3$ Nanocrystals Showing Superior Photoluminescence: Nonstoichiometry Induced Transformation and Light-Emitting Applications, *Adv. Funct. Mater.*, 2018, **28**, 1–7.

28 M. Liu, J. Zhao, Z. Luo, Z. Sun, N. Pan, H. Ding and X. Wang, Unveiling Solvent-related effect on Phase Transformations in CsBr-$PbBr_2$ System: Coordination and Ratio of Precursors, *Chem. Mater.*, 2018, **30**, 5846–5852.

29 F. Palazon, G. Almeida, Q. A. Akkerman, L. De Trizio, Z. Dang, M. Prato and L. Manna, Changing the Dimensionality of Cesium Lead Bromide Nanocrystals by Reversible Postsynthesis Transformations with Amines, *Chem. Mater.*, 2017, **29**, 4167–4171.

30 J. Lin, M. Lai, L. Dou, C. S. Kley, H. Chen, F. Peng, J. Sun, D. Lu, S. A. Hawks and C. Xie, Thermochromic halide perovskite solar cells, *Nat. Mater.*, 2018, **17**, 261–267.

31 Q. A. Akkerman, S. Park, E. Radicchi, F. Nunzi, E. Mosconi, F. De Angelis, R. Brescia, P. Rastogi, M. Prato and L. Manna, Nearly Monodisperse Insulator Cs_4PbX_6 (X = Cl, Br, I) Nanocrystals, Their Mixed Halide Compositions, and Their Transformation into $CsPbX_3$ Nanocrystals, *Nano Lett.*, 2017, **17**, 1924–1930.

32 T. Xuan, S. Lou, J. Huang, L. Cao, X. Yang, H. Li and J. Wang, Monodisperse and brightly luminescent $CsPbBr_3$/Cs_4PbBr_6 perovskite composite nanocrystals, *Nanoscale*, 2018, **10**, 9840–9844.

33 L. Gong, F. Huang, Z. Zhang, Y. Zhong, J. Jin, K.-Z. Du and X. Huang, Multimode dynamic luminescent switching of lead halide hybrids for anti-counterfeiting and encryption, *Chem. Eng. J.*, 2021, **424**, 130544.

34 Q. Q. He, C. K. Zhou, L. J. Xu, S. J. Lee, X. S. Lin, J. Neu, M. Worku, M. Chaaban and B. W. Ma, Highly Stable Organic Antimony Halide Crystals for X-ray Scintillation, *ACS Mater. Lett.*, 2020, **2**, 633–638.

35 Z. P. Wang, J. Y. Wang, J. R. Li, M. L. Feng, G. D. Zou and X. Y. Huang, $[Bmim]_2SbCl_5$: A Main Group Metal-Containing Ionic Liquid Exhibiting Tunable Photoluminescence and White-Light Emission, *Chem. Commun.*, 2015, **51**, 3094–3097.

36 M. Owczarek, P. Szklarz, R. Jakubas and A. Miniewicz, $[NH_2(C_2H_4)_2O]MX_5$: a new family of morpholinium nonlinear optical materials among halogenoantimonate(III) and halogenobismuthate(III) compounds. Structural characterization, dielectric and piezoelectric properties, *Dalton Trans.*, 2012, **41**, 7285–7294.

37 L. Zhou, J. F. Liao, Z. G. Huang, J. H. Wei, X. D. Wang, H. Y. Chen and D. B. Kuang, Intrinsic Self-Trapped Emission in 0D Lead–Free $(C_4H_{14}N_2)_2In_2Br_{10}$ Single Crystal, *Angew. Chem., Int. Ed.*, 2019, **58**, 15435–15440.

38 B. M. Benin, D. N. Dirin, V. Morad, M. Wörle, S. Yakunin, G. Rainò, O. Nazarenko, M. Fischer, I. Infante and M. V. Kovalenko, Highly Emissive Self-Trapped Excitons in Fully Inorganic Zero-Dimensional Tin Halides, *Angew. Chem., Int. Ed.*, 2018, **57**, 11329–11333.

39 R. Gautier, M. Paris and F. Massuyeau, Exciton Self-Trapping in Hybrid Lead Halides: Role of Halogen, *J. Am. Chem. Soc.*, 2019, **141**, 12619–12623.

40 V. Morad, Y. Shynkarenko, S. Yakunin, A. Brumberg, R. D. Schaller and M. V. Kovalenko, Disphenoidal Zero-Dimensional Lead, Tin, and Germanium Halides: Highly Emissive Singlet and Triplet Self-Trapped Excitons and X-ray Scintillation, *J. Am. Chem. Soc.*, 2019, **141**, 9764–9768.

41 A. Getsis and A. V. Mudring, Imidazolium based ionic liquid crystals: structure, photophysical and thermal behaviour of C(n)mim Br center dot xH(2)O (n=12, 14; x=0, 1), *Cryst. Res. Technol.*, 2008, **43**, 1187–1196.

42 A. Paul, P. K. Mandal and A. Samanta, On the Optical Properties of the Imidazolium Ionic Liquids, *J. Phys. Chem. B*, 2005, **109**, 9148–9153.

43 G. Blasse, Luminescence of inorganic solids: from isolated centres to concentrated systems, *Prog. Solid State Chem.*, 1988, **18**, 79–171.

44 Z. Wang, D. Xie, F. Zhang, J. Yu, X. Chen and C. P. Wong, Controlling Information Duration on Rewritable Luminescent Paper Based on Hybrid Antimony(III)

Published on 26 March 2025. Downloaded on 5/31/2026 6:15:04 AM.

Chloride/Small-Molecule Absorbates, *Sci. Adv.*, 2020, **6**, eabc2181.

45 T. V. Sedakova, A. G. Mirochnik and V. E. Karasev, Structure and luminescence properties of antimony(III) complex compounds, *Opt. Spectrosc.*, 2008, **105**, 517–523.

46 C. Sun, Z. Deng, Z. Li, Z. Chen, X. Zhang, J. Chen, H. Lu, P. Canepa, R. Chen and L. Mao, Achieving Near-unity Photoluminescence Quantum Yields in Organic-Inorganic Hybrid Antimony(III) Chlorides with the [SbCl5] Geometry, *Angew. Chem.*, 2023, **135**, e202216720.

47 G. Blasse, G. J. Dirksen and W. Abriel, The influence of distortion of the Te(IV) coordination octahedron on its luminescence, *Chem. Phys. Lett.*, 1987, **136**, 460–464.

48 Z. Wang, D. Huang, Y. Liu, H. Lin, Z. Zhang, A. Ablez, T. Zhuang, K. Du, J. Li and X. Huang, Vacancy Effect on the Luminescent and Water Responsive Properties of Vacancy-Ordered Double Perovskite Derivatives, *Angew. Chem., Int. Ed.*, 2024, **63**, e202412346.

49 C. Zhang, B. Wang, W. Li, S. Huang, L. Kong, Z. Li and L. Li, Conversion of invisible metal-organic frameworks to luminescent perovskite nanocrystals for confidential information encryption and decryption, *Nat. Commun.*, 2017, **8**, 1138.

50 D. Zhang, W. Zhou, Q. Liu and Z. Xia, $CH_3NH_3PbBr_3$ Perovskite Nanocrystals Encapsulated in Lanthanide Metal-Organic Frameworks as a Photoluminescence Converter for Anti-Counterfeiting, *ACS Appl. Mater. Interfaces*, 2018, **10**, 27875–27884.

51 C. Sun, S. Su, Z. Gaop, H. Liu, H. Wu, X. Shen and W. Bi, Stimuli-Responsive Inks Based on Perovskite Quantum Dots for Advanced Full-Color Information Encryption and Decryption, *ACS Appl. Mater. Interfaces*, 2019, **11**, 8210–8216.

52 C. Sun, Z. Gao, H. Liu, L. Wang, Y. Deng, P. Li, H. Li, Z.-H. Zhang, C. Fan and W. Bi, One Stone, Two Birds: High-Efficiency Blue-Emitting Perovskite Nanocrystals for LED and Security Ink Applications, *Chem. Mater.*, 2019, **31**, 5116–5123.

53 J. C. Jin, Y. Z. Wang, K. Han and Z. G. Xia, Rigid phase formation and Sb^{3+} doping of Tin(IV) halide hybrids toward photoluminescence enhancement and tuning for anti-counterfeiting and information encryption, *Angew. Chem., Int. Ed.*, 2024, **63**, e202408653.

54 X. Q. Zhou, S. Zhang, K. Han, J. C. Jin, Y. Sun and Z. G. Xia, Heterovalent doping in $CsCdCl_3$ enabled tunable multimode luminescence and photochromism toward multilevel anti-counterfeiting, *Adv. Opt. Mater.*, 2024, **12**, 2302429.

55 G. J. Zhou, Y. L. Mao, J. Zhang, Q. Q. Ren, M. S. Molokeev, Z. G. Xia and X.-M. Zhang, Dynamic phosphorescence/fluorescence switching in hybrid metal halides toward time-resolved multi-level anti-counterfeiting, *Adv. Funct. Mater.*, 2025, **35**, 2413524.

 This journal is © the Partner Organisations 2025